Nanoparticle assisted magnetic resonance imaging of the early reversible stages of amyloid β self-assembly†

Jin-sil Choi,[a] Hyuck Jae Choi,[b] Dae Chul Jung,[b] Joo-Hyuk Lee[b] and Jinwoo Cheon*[a]

Received (in Cambridge, UK) 26th February 2008, Accepted 19th March 2008
First published as an Advance Article on the web 11th April 2008
DOI: 10.1039/b803294g

Co@Pt–Au nanoparticles, which have enhanced magnetism and high stability in aqueous media, are utilized in conjunction with MRI to monitor the structural evolution of Aβ assemblies, especially Aβ protofibrils in the early reversible stages.

Self-assembly is a term used to describe the spontaneous and intermolecular force-driven organization of components into ordered structures. Processes of this type play crucial roles in cellular functions, and in the construction of higher level structures, such as lipid bilayers in cell membranes, double helical DNA and proteins in quaternary structures.[1] In particular, self-assembly of the amyloid β (Aβ) peptide, leading to malfunction of the neural system, is a known pathogenic process in Alzheimer's disease.[2] Recently, Au nanoparticles have been successfully employed for the highly sensitive detection of Aβ assemblies in optical sensing or bio-bar code systems.[3]

In a magnetic resonance imaging (MRI)-based sensing system, advantage is taken of the fact that the assembly of magnetic nanoparticles in aqueous solution leads to a change in the proton nuclear spin–spin relaxation time ($T2$) of water molecules.[4] Consequently, when used as probes for dynamic biological phenomena, $\Delta T2$ values serve as indicators of not only the switching of magnetic nanoparticles between dispersed and assembled states, but also the degree of assembly of target molecules. In order to maximize MRI signal enhancing effects, nanoparticles with strong magnetism are desirable.[5] Although ferromagnetic metals, such as Fe, Co, and Ni, possess stronger magnetic moments than that of currently widely used iron oxide nanoparticles, they cannot be directly used for biological applications due to their high reactivity in aqueous environments.[6] In this study, we have developed highly stable metal-based heterodimer nanoparticles, which have both large magnetic moments and high colloidal stability. We have used them as probes for direct MRI observation of Aβ assemblies at early stages of the progressive assembly.

The heterodimer nanoparticles, consisting of a Co magnetic core and a Pt shell that is directly fused to an Au nanoparticle (Fig. 1(a)), are prepared from Co@Pt nanoparticles.[7] Au is then deposited on the Co@Pt nanoparticles *via* hydrogenation of $AuCl(PPh_3)$ by purging with a 4% H_2/Ar mixture.[8] The Co@Pt–Au nanoparticles obtained in this manner have a heterodimer structure of roughly 15 nm, composed of 6 nm Co@Pt and 9 nm Au (Fig. 1(b)). The measured face-centered cubic (111) lattice distances of the Pt shell and Au deposition are 2.2 and 2.4 Å respectively, which are consistent with known values[9] (Fig. 1(d)). From energy dispersive X-ray spectroscopic (EDS) analysis, compositional changes corresponding to the Pt (shell), Co (core) and Au clearly confirm the formation of Co@Pt–Au nanoparticles (Fig. 1(d)). Co@Pt and Co@Pt–Au nanoparticles possess almost identical

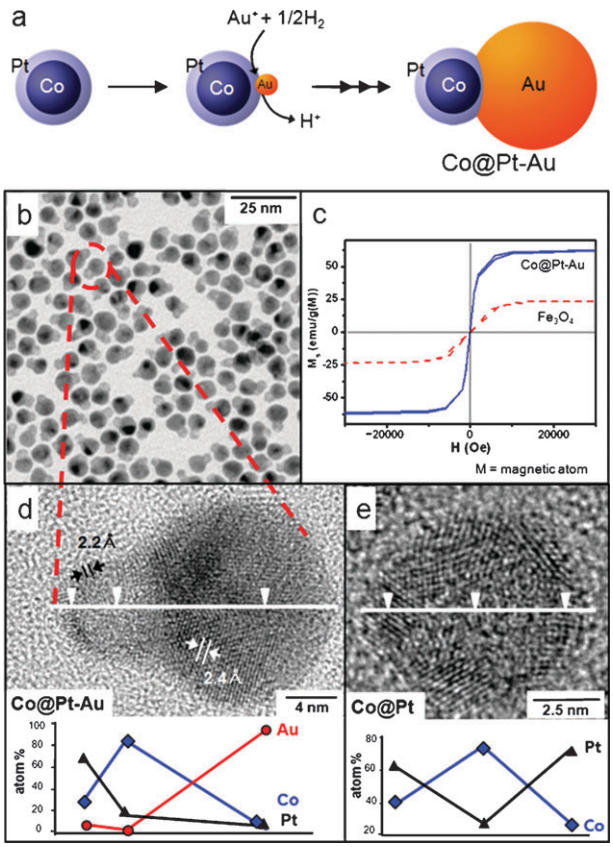

Fig. 1 (a) Schematic of Co@Pt–Au nanoparticle synthesis. (b) Transmission electron microscopy (TEM) image of Co@Pt–Au. (c) Comparison of magnetization per mass of magnetic component of Co@Pt–Au (Co: 4 nm; blue solid line) with 4 nm-sized iron oxide (red dashed line). High resolution TEM (HRTEM) images and composition analysis of (d) Co@Pt–Au and (e) Co@Pt at different spot positions of nanoparticles using EDS (Co: ◆, Pt: ▲, Au: ●).

[a] *Department of Chemistry, Yonsei University, Seoul, 120-749, Korea. E-mail: jcheon@yonsei.ac.kr*
[b] *Department of Radiology, National Cancer Center, Goyang, 410-769, Korea*

† Electronic supplementary information (ESI) available: Experimental details on the fabrication of Co@Pt–Au, conjugation of Co@Pt–Au with NTV, preparation of $A\beta_{40}$ solutions and disassembly of $A\beta_{40}$ under diluted conditions. See DOI: 10.1039/b803294g

magnetization values (63 emu g^{-1} (Co) at 3 T), which are roughly 2.6 times larger than that of identically sized iron oxide nanoparticles (4 nm; 24 emu g^{-1} (Fe))[10] (Fig. 1(c)). For MRI purposes, it is beneficial to have a large magnetism (μ), such as that seen with the Co@Pt–Au nanoparticles, since $\Delta T2$ caused by aggregation is strongly dependent on the magnitude of μ.[5] In addition, the Pt shell of the Co@Pt–Au nanoparticles serves as a protective layer to prevent oxidation of the Co to form antiferromagnetic CoO or Co_3O_4.[7]

To obtain high colloidal stability and target specificity, LA-PEG_{600}-X (LA = lipoic acid, X = OH or COOH)[11] complexes with disulfide ends that bind to the Au surface were ligated to the Co@Pt–Au nanoparticles. With this surface modification, the nanoparticles are stable in solutions containing up to a 2 M salt concentration and over a 1–11 pH range (ESI†). The COOH group of the ligand allows for covalent attachment of bio-active molecules needed for the selective recognition of target molecules. In this study, neutravidins (NTV), which have strong interaction with biotin ($K_a = 10^{-15}$ M), are attached to the Co@Pt–Au nanoparticles (Scheme 1).

Structural changes of Aβ assemblies are dependent upon the concentrations of the initial peptide precursors.[12] It has been proposed that Aβ peptides initially self-assemble to form 2–5 nm-sized oligomers, which then assemble further to form linear-shaped protofibrils (Fig. 2(a)). Upon dilution, both the oligomer and protofibril forms of Aβ peptides can undergo reversible disassembly.[12] When present in higher concentrations, Aβ peptides form larger-sized fibrils, which retain their assembled structures regardless of concentration. These fibrils finally become Aβ plaques.

In this study, the self-assembly processes of $A\beta_{40}$ peptides were monitored using MRI after introducing Co@Pt–Au–NTV nanoparticles. The nanoparticle probes (10 μmol (Co)) were added to 200 μl solutions of various concentrations (0, 0.5, 1, 5, 10, 32, 80 and 250 μM) of the biotinylated $A\beta_{40}$ peptides (Biosource, CA, USA), which had been aged for 2 d to form $A\beta_{40}$ assemblies.[12] Measurements of the $T2$ weighted spin echo MRI signals of these samples show that significant contrast changes take place. The changes in $T2$ range from white to grey and through to black as the $A\beta_{40}$ concentration increases (Fig. 2(b,i)). The color coded images of $T2$ weighted signals more clearly depict the changes taking place (Fig. 2(b,ii)).

The $\Delta T2$ values are the relaxation time differences between solutions containing Co@Pt–Au–NTV mixed with $A\beta_{40}$ assemblies and those containing dispersed Co@Pt–Au nanoparticles in the absence of $A\beta_{40}$ peptides ([$A\beta_{40}$] = 0 μM). The changes in

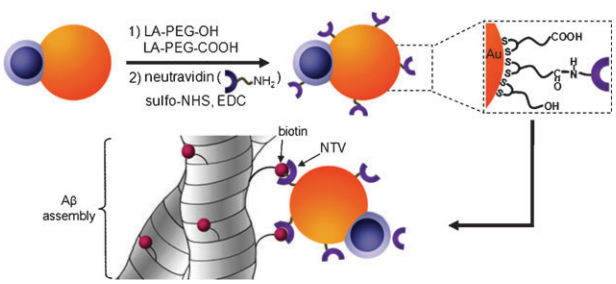

Scheme 1 Schematic of the surface modification of Co@Pt–Au nanoparticles and further conjugation with NTV for the recognition of biotinylated $A\beta_{40}$ assemblies.

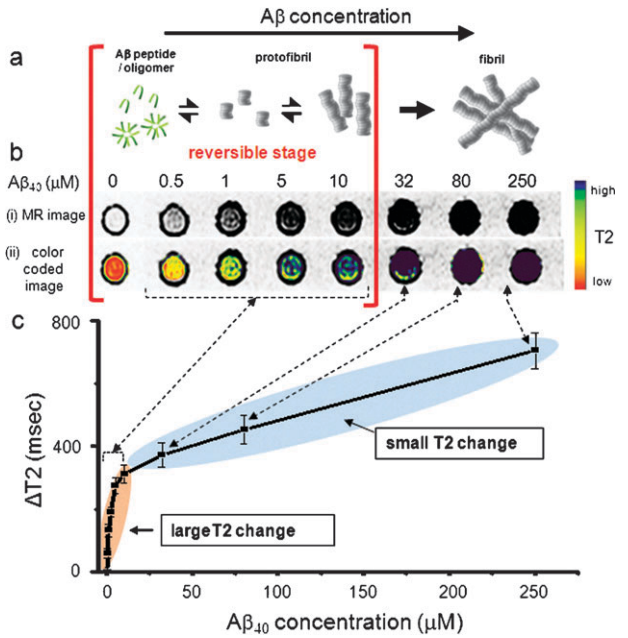

Fig. 2 (a) Schematic of concentration dependent progressive formation of Aβ peptide assemblies. Aβ peptides form reversible assemblies of oligomers and protofibrils through to irreversible assemblies of fibrils. (b, c) $T2$ weighted spin echo MR measurement of Co@Pt–Au solutions with various concentrations of biotinylated $A\beta_{40}$ assemblies. After addition of Co@Pt–Au–NTV probe, (b) $T2$ weighted spin echo MR images (i) and their color coded images (ii) show immediate signal changes, depending on $A\beta_{40}$ structure. (c) In the graph of $\Delta T2$ *vs.* $A\beta_{40}$ concentration, a large $T2$ signal change is observed at the early stages of $A\beta_{40}$ assembly, whereas a small $T2$ signal change is observed at $A\beta_{40}$ concentrations over 10 μM.

$\Delta T2$ are highly susceptible to structural changes taking place in the $A\beta_{40}$ self-assemblies. The MRI measurements show that $\Delta T2$ values are 55.9, 132.1, 275.0, 311.6, 371.7, 454.1 and 704.7 ms for $A\beta_{40}$ concentrations of 0.5, 1, 5, 10, 32, 80 and 250 μM, respectively. The plot of $\Delta T2$ *vs.* $A\beta_{40}$ concentration contains two different slopes, corresponding to a sharp increase in $\Delta T2$ at $A\beta_{40}$ concentrations below 10 μM and a more gradual increase in $\Delta T2$ at higher concentrations (Fig. 2(c)).

The results of concurrent TEM and dynamic light scattering (DLS) studies confirm that structural changes to the $A\beta_{40}$ assembly take place when the $A\beta_{40}$ concentration is incrementally increased (Fig. 3). Implementation of these techniques shows that, in the absence of $A\beta_{40}$ peptides, free Co@Pt–Au nanoparticles are dispersed and non-aggregated, with an approximate hydrodynamic size of 20 nm. At a *ca.* 0.5 μM concentration of $A\beta_{40}$, short 120 nm protofibrils conjugated with a few (2 or 3) Co@Pt–Au nanoparticles begin to appear. The $A\beta_{40}$ protofibrils begin to elongate (140 nm), and more nanoparticles (6–9) become attached as the $A\beta_{40}$ concentration is increased to 5 μM. At a concentration of 80 μM, highly irregularly-shaped $A\beta_{40}$ assemblies of roughly 1.2 μm hydrodynamic size are produced.

The observed changes in $\Delta T2$ are well correlated with the assembly patterns of $A\beta_{40}$ peptides. This is especially true at the early stages of assembly, where a large $\Delta T2$ is observed. This finding indicates that MRI is sensitive to the structural

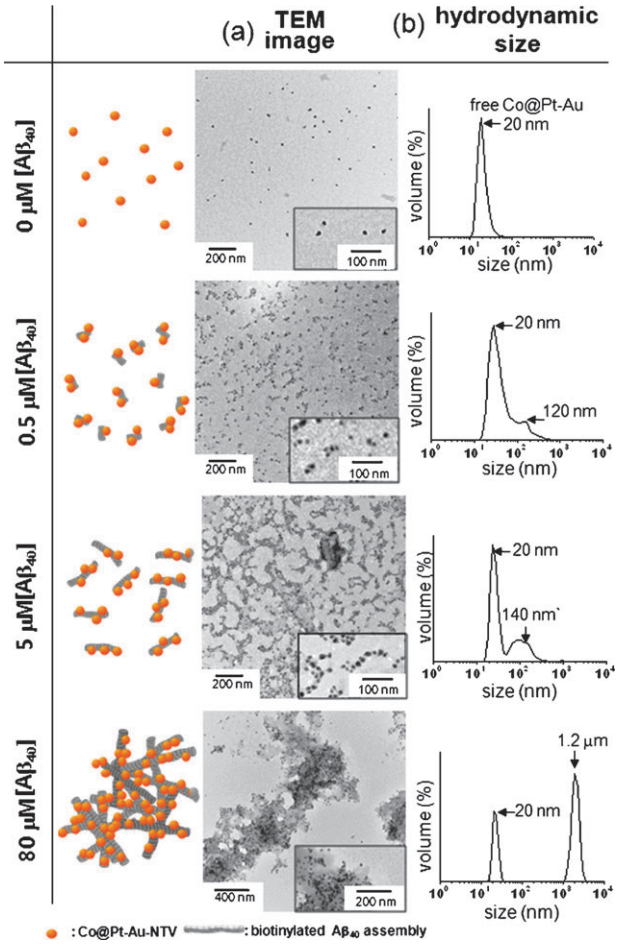

Fig. 3 Co@Pt–Au–NTV nanoparticle aggregates induced by $A\beta_{40}$ assemblies. (a) TEM and magnified TEM images (inset) show progressive structural changes of nanoparticle assemblies, depending on $A\beta_{40}$ concentration (0, 0.5, 5 and 80 μM). (b) DLS data also show the size changes of Co@Pt–Au–NTV–$A\beta_{40}$ assemblies as the $A\beta_{40}$ concentration increases.

changes taking place at the early stages of assemblies including protofibrils. On the other hand, at $A\beta_{40}$ concentrations over 10 μM, the MRI response to the $A\beta_{40}$ process is not as large.

Early stage protofibrils, with strong *T*2 changes, are in a reversible state. For example, protofibrils that are produced at $A\beta_{40}$ concentrations around 5 μM reversibly disassemble. Only dispersed Co@Pt–Au (hydrodynamic size of ~20 nm) is observed when the protofibrils are diluted to 0.1 μM ($A\beta_{40}$) and kept for 4 d (ESI†). In contrast, fibrils generated at 80 μM ($A\beta_{40}$) maintain their micron-sized irregular aggregate form without a significant change in their size when diluted. Since it is possible to reverse and retard the Aβ assembly process, the ability to detect Aβ assemblies in their reversible stages is important in the context of Alzheimer's disease treatment.[13]

In summary, we have demonstrated that Co@Pt–Au nanoparticles that have enhanced magnetic properties and high colloidal stability can be used in conjunction with MRI to monitor key structural stages of Aβ assemblies. The exceptional, dramatic changes that take place in MR signals during Aβ assembly enable the detection of Aβ protofibrils in the early reversible stages. This is an important finding because information of this type could be used in a therapeutic approach to Alzheimer's disease that involves the reversible disassembly of Aβ protofibrils. Furthermore, the magnetic nanoparticle-assisted MRI detection system could be applied as a sensitive probe of protein self-assemblies including prion, α-synuclein and Huntingtin.

We thank Dr Y.-w. Jun for his helpful discussions and M.-y. Kim for her graphics work. This work is supported in part by NRL (R0A-2006-000-10255), NCI Center for Cancer Nanotechnology Excellence, AOARD (FA4869-07-1-4016), NCRC (R15-2004-024-00000-0), Nano/Bio Science & Technology Program (M10503000218-05M0300-21810), the KRC of Fundamental Science & Technology (2N30630-07-259), the BK 21 Project and Seoul Science Fellowship.

Notes and references

1 D. Philip and J. F. Stoddart, *Angew. Chem., Int. Ed. Engl.*, 1996, **35**, 1154; G. M. Whitesides and B. Grzybowski, *Science*, 2002, **295**, 2418; G. M. Whitesides and M. Boncheva, *Proc. Natl. Acad. Sci. U. S. A.*, 2002, **99**, 4769.
2 Y. Gong, L. Chang, K. L. Viola, P. N. Lacor, M. P. Lambert, C. E. Finch, G. A. Krafft and W. L. Klein, *Proc. Natl. Acad. Sci. U. S. A.*, 2003, **100**, 10417; B. A. Chromy, R. J. Nowak, M. P. Lambert, K. L. Viola, L. Chang, P. T. Velasco, B. W. Jones, S. J. Fernandez, P. N. Lacor, P. Horowitz, C. E. Finch, G. A. Krafft and W. L. Klein, *Biochemistry*, 2003, **42**, 12749.
3 D. G. Georganopoulou, L. Chang, J.-M. Nam, C. S. Thaxton, E. J. Mufson, W. L. Klein and C. A. Mirkin, *Proc. Natl. Acad. Sci. U. S. A.*, 2005, **102**, 2273; A. J. Haes, S. Zou, G. C. Schatz and R. P. Van Duyne, *J. Phys. Chem. B*, 2004, **108**, 109.
4 J. M. Perez, L. Josephson, T. O'Loughlin, D. Hãgemann and R. Weissleder, *Nat. Biotechnol.*, 2002, **20**, 816; C. Kaittanis, S. A. Naser and J. M. Perez, *Nano Lett.*, 2007, **7**, 380; T. J. Harris, G. von Maltzahn, A. M. Derfus, E. Ruoslahti and S. N. Bhatia, *Angew. Chem., Int. Ed.*, 2006, **45**, 3161; J. Wan, W. Cai, X. Meng and E. Liu, *Chem. Commun.*, 2007, 5004; S. A. Corr, A. O' Byrne, Y. K. Gun'ko, S. Ghosh, D. F. Brougham, S. Mitchell, Y. Volkov and A. Prina-Mello, *Chem. Commun.*, 2006, 4474.
5 A. Rocha, Y. Gossuinb, R. N. Mullera and P. Gillis, *J. Magn. Magn. Mater.*, 2005, **293**, 532; N. S. Sobal, U. Ebels, H. Mohwald and M. J. Giersig, *J. Phys. Chem. B*, 2003, **107**, 7351; N. Pazos-Perez, Y. Gao, M. Hilgendorff, S. Irsen, J. Perez-Juste, M. Spasova and M. Farle, *Chem. Mater.*, 2007, **19**, 4415.
6 A.-H. Lu, E. L. Salabas and F. Schuth, *Angew. Chem., Int. Ed.*, 2007, **46**, 1222; B. D. Cullity, in *Introduction to Magnetic Materials*, ed. M. Cohen, Addison-Wesley Pub. Co., Reading, MA, USA, 1972, ch. 4, pp. 117.
7 J.-I. Park and J. Cheon, *J. Am. Chem. Soc.*, 2001, **123**, 5743; Y.-w. Jun, J.-s. Choi and J. Cheon, *Chem. Commun.*, 2007, 1203; C.-H. Jun, Y. J. Park, Y.-R. Yeon, J.-r. Choi, W.-r. Lee, S.-j. Ko and J. Cheon, *Chem. Commun.*, 2006, 1619.
8 J.-s. Choi, Y.-w. Jun, S.-I. Yeon, H. C. Kim, J.-S. Shin and J. Cheon, *J. Am. Chem. Soc.*, 2006, **128**, 15982.
9 JCPDS card numbers are 01-1311 for Pt and 02-1095 for Au.
10 Y.-w. Jun, Y.-M. Huh, J.-s. Choi, J.-H. Lee, H.-T. Song, S.-j. Kim, S. Yoon, K.-S. Kim, J.-S. Shin, J.-S. Suh and J. Cheon, *J. Am. Chem. Soc.*, 2005, **127**, 5732; J.-I. Park, Y.-w. Jun, J.-s. Choi and J. Cheon, *Chem. Commun.*, 2007, 5001.
11 H. T. Uyeda, I. L. Medintz, J. K. Jaiswal, S. M. Simon and H. Mattoussi, *J. Am. Chem. Soc.*, 2005, **127**, 3870; M. Hans, K. Shimoni, D. Danino, S. J. Siegel and A. Lowman, *Biomacromolecules*, 2005, **6**, 2708.
12 J. D. Harper, S. S. Wong, C. M. Lieber and P. T. Lansbury, Jr., *Biochemistry*, 1999, **38**, 8972; G. Bitan, M. D. Kirkitadse, A. Lomakin, S. S. Bollers, G. B. Bennedek and D. B. Teplow, *Proc. Natl. Acad. Sci. U. S. A.*, 2003, **100**, 330.
13 W. L. Klein, G. A. Krafft and C. E. Finch, *Trends Neurosci.*, 2001, **24**, 219; J. Suh, S. H. Yoo, M. G. Kim, K. Jeong, J. Y. Ahn, M.-s. Kim, P. S. Chae, T. Y. Lee, J. Lee, J. Lee, Y. A. Jang and E. H. Ko, *Angew. Chem., Int. Ed.*, 2007, **46**, 7064.